Original Scientific Paper

Istraživanja i projektovanja za privredu
Journal of Applied Engineering Science

doi:10.5937/jaes0-27589

Paper number: x(yyyy)z, XXX, xxx-xxx

A GREEN AND LOW-COST OF MESOPOROUS ELECTRODE BASED ACTIVATED CARBON MONOLITH DERIVED FROM FALLEN TEAK LEAVES FOR HIGH ELECTROCHEMICAL PERFORMANCE

Erman Taer[1], Miftah Ainul Mardiah[1], Agustino[1], Widya Sinta Mustika[1], Apriwandi[1], Rika Taslim[2]*

[1]Universitas Riau, Faculty of Mathematic and Natural Science, Department of Physics, Pekanbaru, Indonesia

[2]Islamic State University of Sultan Syarif Kasim, Faculty of Science and Technology, Departement of Industrial Engineering, Pekanbaru, Indonesia

Mesoporous carbon materials derived from the novel biomass of fallen teak leaves were synthesized using versatile, low cost, and environmentally friendly route. Therefore, mesoporous carbon materials were prepared in the monolith form, followed by treatment with the integrated pyrolysis of both carbonization and physical activation. In addition, there are detailed studies and analysis on the influences of chemical activation processes under different concentrations on the textural properties, morphology, crystalline degree, chemical elements and electrochemical performance. These mesoporous carbon possess the highest specific surface area of 489.81 $m^2 g^{-1}$, with a pore volume of 0.293 $cm^3 g^{-1}$, and well-developed mesoporosity. Hence, the electrode of mesoporous carbon for supercapacitor in two electrode system with 1 M H_2SO_4, exhibits a high specific capacitance of 280 F g^{-1} without heteroatom doping. This report provides an effective route to utilize the novel biomass of fallen teak leaves, with the potential benefits of waste reduction and the production of excellent electrode to serve as energy storage materials.

Key words: activated carbon, mesoporous, monolith, supercapacitor, teak leaves

INTRODUCTION

Supercapacitors, also known as electrochemical double layer capacitance (EDLC), is an adopted strategy for renewable and sustainable resource required in energy storage, and devoid of mass depletion [1, 2]. This supercapacitors demonstrates a performance between batteries and conventional capacitor integrated with higher power density, fast charge/discharge rate, and prolonged life cycle [3, 4]. However, known applications in the field of portable electronic devices and electric vehicles require subjection to a large energy density estimated to limit speculative value range between 3-5 Wh kg^{-1} [5]. Based on the equation $E_s = 1/2CV^2$, the energy density, is assumed to expand by increasing the specific capacitance (C) or extending the window voltage (V) [6–8]. Under these circumstances, a facility approach is employed to develop quality electrode material targeting this specific capacitance. In EDLC, the specific capacitance is determined by accumulating the ion pairs formed at the interface between electrolyte and polarized electrode which is affected by pore size distribution and accessibility surface specific area [9–11]. Therefore, electrodes with suitable pore structure are prerequisites for enhanced specific capacitance.

Biomass based activated carbon has been widely applied in supercapacitor electrode in large quantity, low cost production, environmentally friendly product, and facile route processing [11–13]. More specially, activated carbon as supercapacitor electrode plays a significant role in electrochemical performance due to high specific surface area, nature micro-meso porosity, active functional group (hydroxyl and carboxyl), and good electrical conductivity [14]. For instance, wood, grass, fruit shell or seeds, and leaves are the major biomass showing potentials precursor for high carbon yield [4, 15, 16]. Moreover, daily leaves dropped causes more waste accumulation with several reports suggesting their usefulness as activated carbon electrode in supercapacitor applications, including acacia [17], albizia procera [18], encalyptus [19], bamboo [20], ginkgo [21], lotus [22], tomato [23], phoenix [24], and willow [25].

Teak leave, for example, is one major plant cultivated in Indonesia, covering a total size of 1.085 million ha, and mostly grown in tropical forest at Java, Sumatera, and Bali island [26]. Furthermore, during dry season, the leaves fall to prevent dehydration, hence contributing to environmental waste. Currently, the teak leaves were reportedly used as supercapacitor electrodes, in which a preliminary investigation showed a specific capacitance of 113Fg^{-1} [27]. Also, there is no other study that promoted teak leaves as raw materials for supercapacitor application.

The electrode is designed as monolith by providing good mechanical stability and high electrical conductivity in order to achieve an improvement in supercapacitor applicability [28]. Additional benefits include the possession of interconnected pore structure generated from micro-meso-macro-porosity linkage. This delivers good accessibility to electrolyte ions [29], and prevents material binding, therefore contributing to higher electrical conductivity and increased specific capacitance [28]. However, the mono-

*erman_taer@yahoo.com

lith is prepared by conforming the mold under pressure with carbon powder followed by carbonization [30, 31]. The route further shows the capacity to design interconnected pore structure, including (I) activation on carbon powder using an activator agent, lead to generate micro-meso-porosity [30]; (II) the mold process provides macro-porosity resulting in interconnected pore structure [17].

This research involves the synthesis of activated carbon monolith with mesopore texture from fallen teak leaves waste for developing supercapacitor electrodes. The sample was prepared through integrated pyrolysis (carbonization and physical activation), and assisted with chemically activation using potassium hydroxide (KOH) under various concentration (i.e., 0.2M and 0.4M). The physical characteristic was examined using N_2 sorption, XRD, EDX, SEM, to evaluate those characteristic as the influence on the electrochemical performance. Cyclic voltammetry (CV) was used to evaluate the electrochemical performance, which was operated in 1M H_2SO_4 electrolyte for low voltage between 0.0-0.5V. Density parameter of activated carbon monolith will be discussed in detail. Also, thermal analysis was done using TGA, and it will be discussed.

EXPERIMENTAL METHODS

Electrode preparation

Teak leaves (TL) waste were collected in the University of Riau, Pekanbaru, Riau province, Indonesia and synthesized into activated carbon monolith using the steps earlier specified (Figure 1); (1) This involved the conversion teak leave into powder, through ball milling 20 hours and sieving into a size of ≤ 53μm; (2) Subsequently, the resulting powder was chemically activated by applying potassium hydroxide (KOH) under various concentration (i.e., 0.2M and 0.4M).

Then, the activated carbon was molded using hydraulic press by a constant mass loaded of 8 ton, to achieve a monolith form in coin-shaped with diameter size of ~2cm; (4) Furthermore, the samples were carbonized at a temperature of 600°C through an N_2 gas atmosphere, followed by a physical activation with temperature of 850°C for 2 hours in a CO_2 gas atmosphere. In detail, this method has been reported in patents with a number of P00201810426 [32]. Subsequently, the entire samples were polished and washed with deionized water to achieve a neutral pH. Finally, the complete process converted the leaves into activated carbon monolith, as represented by ACMTLx, where x refers to KOH concentration.

Physical characterization

The effects of thermal treatment on the TL sample were evaluated at a temperature range from 30-600°C using thermogravimetric analysis (TGA, Shimadzu TGA-50). In addition, the density was calculated from mass (digital scales Labtronics), diameter and thickness (electronic Caliper Insize Series 1112) of 10 electrodes to observe preliminary porosity at ACMTLx. The textural characteristics, including the specific surface area due to Brunauer-Emmett-Teller (BET) model, were analyzed by the N_2 gas sorption (Quantachrome TouchWin v1.2 instrument). Also, the mesopore volume and pore size distribution were determined through the Barret-Joiner-Halenda (BJH) method; where the total volumes were estimated from the amount of absorbed nitrogen at a relative pressure of ~0.95. Furthermore, the scanning electron microscopy (SEM, JEOL-JSM-6510LA) and embedded energy X-ray (EDX) were used to observe the morpholo-

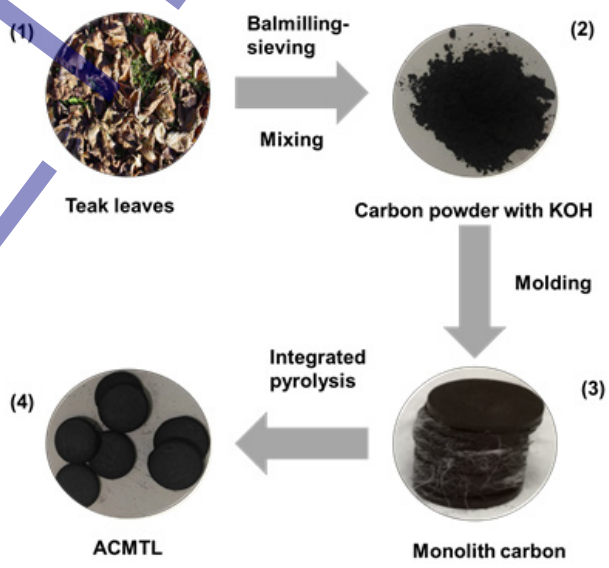

Figure 1: Schematic in ACMTL production

gy structure and chemical elements, respectively. These assessments were conducted on monolith form without coating, although an accelerating voltage of 15kV was applied.

The X-ray diffraction (XRD, X-Pert Pro PW3060/10) with a source of Cu-Kα radiation (Kα=1.5418 Å) was used to define the crystalline degree of the carbon electrodes. This assessment was analyzed in a 2θ scale range of 10-100°, while the interlayer *d* spacing (d_{002} and d_{100}) was calculated with the Bragg's Law, as determined from equation (1). Meanwhile, the micro-crystallite dimensions, including average crystalline thickness (L_c) and graphene sheet diameter (L_a), were evaluated as turbostratic crystallites structure, using empirical expression by Debey-Scherer from equations (2) and (3). The number of graphitic layers (N) was estimated following equation (4).

$$n\lambda = 2\,d\,sin\theta \quad (1)$$

$$L_c = \frac{0.89\lambda}{\beta cos\ \theta_{002}} \quad (2)$$

$$L_a = \frac{1.94\lambda}{\beta_{cos}\,\theta_{100}} \quad (3)$$

$$N = \frac{L_c}{d_{002}} \quad (4)$$

Where, n is the mean diffraction order in value, with a maximum order of 1, λ denotes the X-ray wavelength for Cu-Kα radiation of 1.5418 Å, while *d* was defined as the interlayer d spacing, where d_{002} and d_{100} signifies θ_{002} and θ_{100}, respectively. Furthermore, θ represents the angle of reflection plane, known as 002 and 100 planes. β is the full width at half-maximum of the plane 2θ, while 2θ denotes the scattering angles (degree).

Electrochemical characterization

Cyclic voltammetry (CV, UR Rad-Er 5841 instrument) was extensively used to analyze the electrochemical behavior in a two electrode system, where the voltage applied ranged between 0.0V-0.5V. Meanwhile, supercapacitor cells was assembled in a symmetrical layer, comprised of electrodes (ACMTL), electrolyte (1M H_2SO_4), separator (duck eggshell) [33], current collector (stainless steel 316L), isolator (teflon), and body cells (acrylic). Subsequently, the electrochemical behavior was evaluated in terms of the specific capacitance, energy and power densities using equations (5), (6), and (7), consecutively.

$$C_{sp} = \frac{Ic - Id}{sxm} \quad (5)$$

$$E_s = \frac{1}{2}CV^2 \quad (6)$$

$$P_s = \frac{E_s}{\Delta t} \quad (7)$$

Where I_c is the charging current (A), I_d is the discharge current (A), *s* is the scan rate (mV s^{-1}) and *m* is the mass of the electrode (g). Furthermore, E_s is the energy density (Wh kg^{-1}), C_{sp} is specific capacitance (F g^{-1}), *V* is cell voltage (V), P_s is power density (W kg^{-1}), and Δ_t is discharge time (s).

RESULTS AND DISCUSSIONS

Thermal analysis

Figure 2 shows the supramolecular properties of teak leaves derived from carbon materials that was investigated using thermogravimetric analysis (TGA). The results indicated possible plant decomposition leading to changes in the polymer structure (cellulose, hemicellulose, and lignin) to carbon atom in the form of released oxygen and hydrogen. This discharge occurred during heat treatment, after the water content had initially vaporized at a specified temperature of 98.1°C. Although, the biomass samples generally decomposed at a temperature range of 272–372°C, estimated at 45.87%. However, the data corresponds to hemicellulose decomposition for temperatures between 200-580°C [34], while 240–350°C was reported for cellulose. Finally, the TG curve recorded maximum weight loss of the teak leaves of 62.55% at a temperature of 560.5°C, similar to lignin degradation at a temperature range of 200–800°C [15]. Based on the DTG curve, highest disintegration was obtained at a rate of 0.472mg/min, in line with the proposition for fixed carbonization temperatures. These data are potentially applied in an effort to achieve considerable carbon yield and low volatility during the teak leaves production.

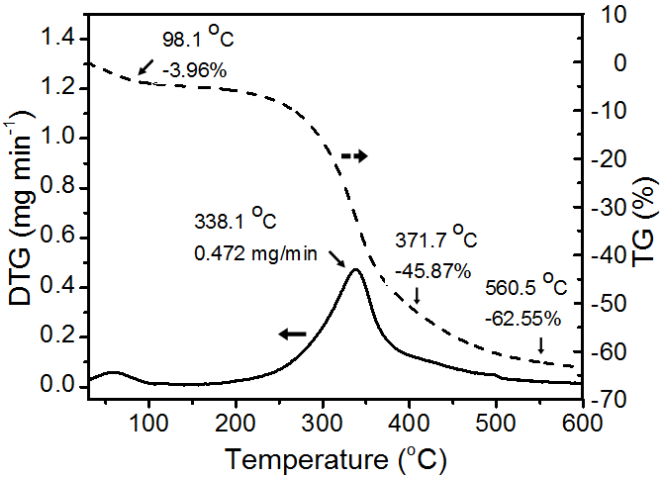

Figure 2: Supramolecular characteristic changes characterized using TGA

Density

Figure 3 specifies the density of the ACMTLx samples prior to the carbonation-activation process decreases from 0.86g cm^{-3} to 0.77g cm^{-3} and 0.85g cm^{-3} to 0.68g cm^{-3} for ACMTL0.2 and ACMTL0.4, respectively. This was attributed to the release of certain volatile elements, including oxygen, hydrogen, and nitrogen, as well as the introduction

of CO_2 produced carbon monoxide and hydrogen. Under these circumstances, some vacancies and carbon restructuring were observed, resulting to mass and volume reduction [35]. Subsequently, the ACMTL0.4 acquired lower density compared to ACMTL0.2 due to better pore generation on carbon electrode at higher KOH concentration. The condition generally indicates a highly amorphous structure and larger porosity. Meanwhile, the Romero-Rangel model reported an applied density of 0.75g cm^{-3} produces a sponge-like nanoporous carbon structure. Also, these specifications are assumed to provide extensive electronic charge transfer in ion improvement and carbon surface interaction [36].

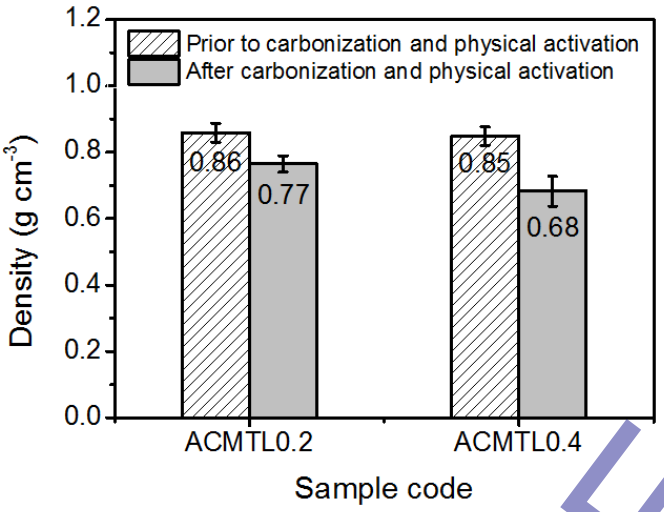

Figure 3: Density of ACMTLx samples

N_2 sorptions

Figure 4(a) represents N_2 adsorption/desorption isotherms from ACMTLx. The activated carbon pore size is characterized by three types, including micropore (<2nm), mesopore (2-50nm), and macropore (>50nm)[37], based on the International Union of Pure and Applied Chemists (IUPAC) classification. These lines disclosed a hysteresis loop at relatively high pressure (P/P_0=0.4-0.8) corresponding to type IV mesopores. Also, the isotherms significantly shows an adsorption volume rate of lower relative pressure (P/P_0<0.2), indicating micropore formation [38]. Figure 4(b) highlights the BJH (Barrett-Joyner-Halenda) model that was employed to evaluate the pore size distribution. This describes the samples acquired pore sizes in the form of mesopores (D_{BJH}), with diameters of 3.562nm (ACMTL0.2) and 3.558nm (ACMTL0.4).

Table 1 reflects a summary of the textural properties of ACMTLx samples, where an increase in KOH concentration enhances the specific surface area (SBET), the mesopore surface (SBJH) and volume (VBJH), as well as the total pore (VTOTAL) and average diameter of pore (Daverage). Subsequently, the porous carbon was achieved through chemical and physical activation [39]. Chemically activation of KOH generated porous carbon by intercalating K+ into carbon [40]. The potassium hydroxide was initially decomposed to produce potassium carbonate at temperature of 600°C, and it also formed micropores (Equation 8). Further breakdown at temperature above 700°C, the carbonates was converted into carbon dioxide and more micropores was developed. However, strong acid etching instigated more mesopores (Equation 9), hence, the potassium carbonate completely degraded at a temperature of 800°C. The carbon dioxide combined with carbon to form carbon monoxide with the

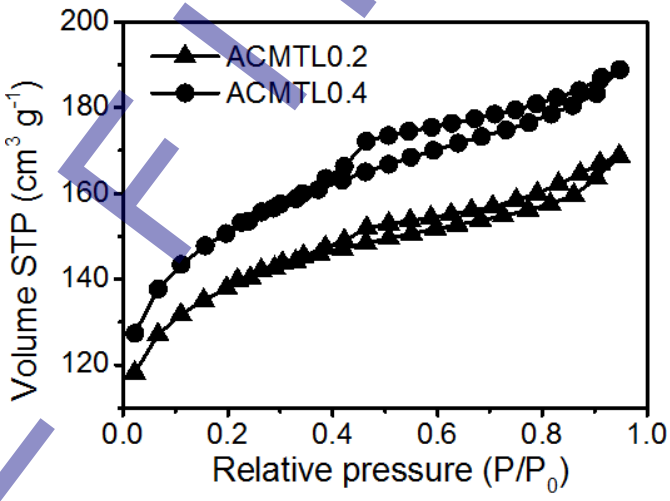

(a)

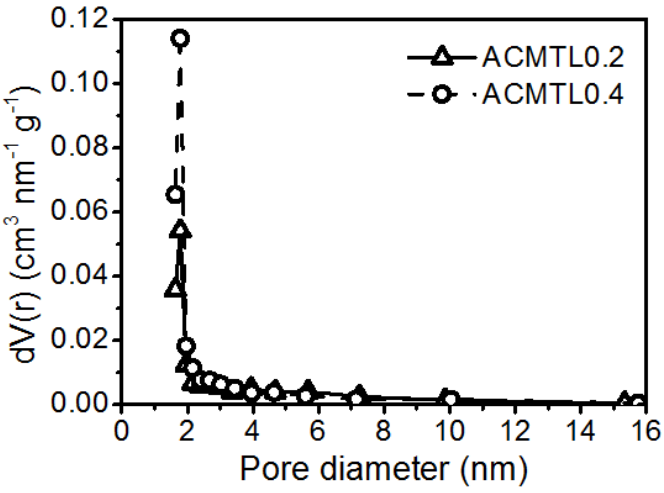

(b)

Figure 4: a) Nitrogen adsorption-desorption isotherms, b), and pore size distribution

Table 1: Textural properties of ACMTLx samples

Samples	S_{BET} (m^2g^{-1})	S_{BJH} (m^2g^{-1})	V_{TOTAL} (cm^3g^{-1})	V_{BJH} (cm^3g^{-1})	D_{BJH} (nm)	Daverage (nm)
ACMTL0.2	444.336	32.216	0.262	0.049	3.562	2.356
ACMTL0.4	489.806	49.920	0.293	0.064	3.558	2.392

opening of previous inaccessible pores due to disordered carbon atom and heteroatom. The existing micropores were continuously enlarged by collapsing the surrounding adjacent walls. In addition, the potassium compounds (K_2O and K_2CO_3) bonded with carbon at a temperature range of 800-900°C, to produce metallic potassium (K) and carbon monoxide (CO) (Equation 11-13), where the K^+ ion were removed from carbon lattice by washing [40].

$$6KOH + 2C \rightarrow 2K + 3H_2 + 2K_2CO_3 \quad (8)$$

$$K_2CO_3 \rightarrow CO_2 + K_2O \quad (9)$$

$$CO_2 + C \rightarrow 2CO \quad (10)$$

$$K_2CO_3 + 2C \rightarrow 2K + CO \quad (11)$$

$$K_2O + C \rightarrow 2K + CO \quad (12)$$

$$K_2O + C \rightarrow C - O - K + K \quad (13)$$

X-ray diffraction (XRD)

Figure 5 shows the crystalline degree of the teak leaves by X-ray diffraction (XRD), where the diffractogram further displayed the ACMTLx samples in two strong peaks at 2θ about 24° and 46° due to the planes (002) and (100). The broad and low intensity peaks indicate the presence of an amorphous carbon structure with low degree of graphitization. Although, ACMTL0.4 possessed slightly larger 2θ on planes (002), suggesting a high disorder carbon attributed to strong alkaline etching. This translates into a higher amorphous carbon state [30]. Meanwhile, some sharp peaks in ACMTLx were observed as by-product of pyrolysis, involving silica dioxide (SiO_2), calcium carbonate ($CaCO_3$), and potassium (K) [31].

The XRD parameters, including interlayer spacing (d_{002} and d_{100}) and micro crystallites dimension (L_c for average crystallite sizes and L_a for average graphene sheets) were continued in Table 2. Interlayer spacing (d_{002}) was calculated from Bragg's formula (equation 1) showing the activated carbon derived teak leaves are larger compared to graphite (d_{002}=3.35Å). This considerably facilitates the electrolyte ion penetration and further improves the electrochemical properties [41]. Also, on average, the crystallite sizes (L_c) and graphene sheets (L_a) were evaluated from equation 3 and 4, respectively. The results showed that the data for ACMTLx is typical range for carbon materials. For examples, the values of L_c and L_a were reported for carbon electrode from rubber wood sawdust synthesized under various KOH concentration in the ranges of 6.358-12.120Å and 6.374-12.333Å, respectively [30]. Activated carbon from mission grass demonstrated L_c and L_a range between 11.158-18.290Å and 8.423-24.566Å, respectively [42]. Moreover, L_c and L_a declined by the addition of concentrated KOH due to strong alkaline etching and carbon atom rearrangement at high temperatures during carbonization and physical activation.

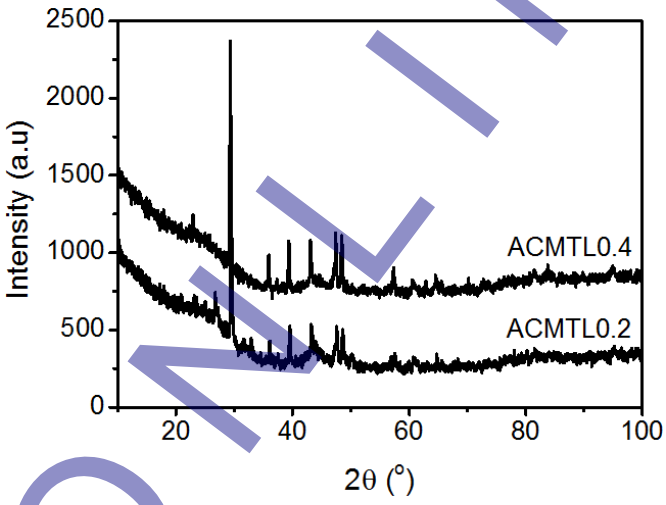

Figure 5: X-ray diffractogram

Further analysis, the data were demonstrated in term of ratio L_c/d_{002} and L_c/L_a, representing the mean number of planes in the micro crystallites (N), and the relative density of the edge and basal planes, respectively. These features are associated with the development of electrode pore structures to further influence the formation of the electric double layer and electrode capacitance [42]. In addition, the data corresponded to the empirical formula applied from previous studies of activated carbon electrode using rayon cloth, as defined in Equation 14.

$$SSA_{xrd} = \frac{2}{\rho_{xrd} L_c} \quad (14)$$

$$\rho_{xrd} = \left(\frac{d_{002(graphite)}}{d_{002}} \right) \rho_{(graphite)} \quad (15)$$

Where SSA_{xrd} is specific surface area prediction (m^2g^{-1}), while $d_{002(graphite)}$ is interlayer spacing of graphite (d_{002}=0.33354nm), and ρ_{xrd} denotes graphite density of carbon samples, also $\rho_{graphite}$ is defined in the value of 2.268g cm^{-3}. The specific surface area generated were 577.90m^2 g^{-1} and 994.23m^2 g^{-1} for ACMTL0.2 and ACMTL0.4, respectively. These data assumed the lower crystallite size (L_c) provides a more better specific surface area, resulting to more ion pairs formation [43].

Energy Dispersive X-ray (EDX)

The chemical elements in the activated carbon derived teak leaves material were observed through an energy dispersive X-ray (EDX), which is resumed in Table 3. The ACMTLx samples mainly contained carbon (C) and oxygen (O), attributed to the degradation of hemicellulose, cellulose, and lignin during carbonization and physical

Table 2: XRD parameters of ACMTLx samples

Samples	2θ (002)	2θ (100)	d_{002} (Å)	d_{100} (Å)	L_c (Å)	L_a (Å)	L_c/L_a	N
ACMTL0.2	24.588	46.097	3.618	1.968	16.559	18.419	0.899	4.577
ACMTL0.4	24.558	47.064	3.622	1.929	9.634	7.479	1.288	2.660

activation [44]. This contributes to carbon and oxygen bonding by the functional group, including phenol group (C-OH) or carboxylic group (COOH) [28]. Although, the oxygen concentration increased due to a steady rise in KOH, while carbon declined as a result of C and O bonding. However, higher oxygen concentration in the sample is assumed to advance the wettability of diffused aqueous electrolyte ions through the deep pore of electrode [45]. Moreover, less amount of volatiles were discovered in the teak leaves derived activated carbon materials [46]. The magnesium (Mg) was attributed to natural mineral originated from biomass depending on initial compositions. Silica (Si) and Calcium (Ca) contributed ash as by-product pyrolysis from silica dioxide (SiO_2) and calcium carbonate ($CaCO_3$). In addition, potassium (K) was supplied by KOH activation referred as potassium carbonate (K_2CO_3), potassium oxide (K_2O), and metallic potassium (K) [28]. The residues were associated to incomplete removal of the compounds [47].

Table 3: Chemical elements of ACMTLx samples

Elements	ACMTL0.2 Mass (%)	ACMTL0.4 Mass (%)
C	79.52	76.53
O	13.25	15.49
Mg	-	0.20
Si	2.31	2.32
K	0.87	1.04
Ca	4.04	4.43
Total	100	100

Scanning electron microscopy (SEM)

Figure 6 shows the surface morphology and nature of porosity of teak leaves derived carbon materials were examined by SEM. The ACMTL0.2 reveals the formation of large size carbon materials with rough surface in the micro-meter size range, as shown in Figure 5(a). This also depicts a unique structure on the materials of an ellipse-liked shape with diameter sizing of 1.18 µm, in addition to the large macropores formed between the carbon particles (Figure 6(b)).

Figure 6(c) indicates the ACMTL0.4 with a reduction rough surface and the formation of larger size carbon particles. This clearly shows that increased KOH concentration accelerates the opening of more amounts of inaccessible macropores, while declining in size. Figure 5(d) shows the formation of larger size carbon particles, contributing to better improvement on specific surface area. Finally, the surface morphology and nature porosity played a significant role in electrochemical performance; I) the macropores serve as transport channels in electrolyte ion diffusion into mesopores and micropores; II) larger number of macropores formed provide better access for electrolyte ion diffusion ; III) larger size formation

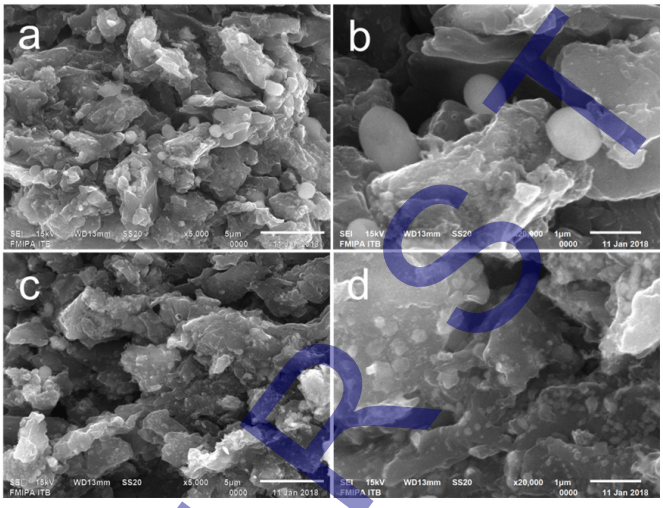

Figure 6: SEM image of teak leaves derived carbon samples; ACMTL0.2 (a-b); ACMTL0.4(c-d)

of carbon particles is assumed to improve accessibility in specific surface area.

Electrochemical performance

The CV measurement was conducted in two electrode system in 1M H_2SO_4 electrolyte with a voltage in the range of 0.0-0.5V, by applying a scan rate parameter of 1mV s^{-1}. Figure 7 shows the ACMTLx curve in the form of rectangular like-shape, translating to an electrical double layer formation in the absence of redox contribution [22]. However, the specific capacitance (C_{sp}) was calculated using Equation 5, estimated to 135 F g^{-1} and 280 F g^{-1} for ACMTL0.2 and ACMTL0.4, respectively. These values are as a result of increased KOH concentration in the electrode features; (I) high porosity through mesopores volume and macropores; (II) improvement in specific surface area and accessibility; (III) an increase in carbon surface wettability.

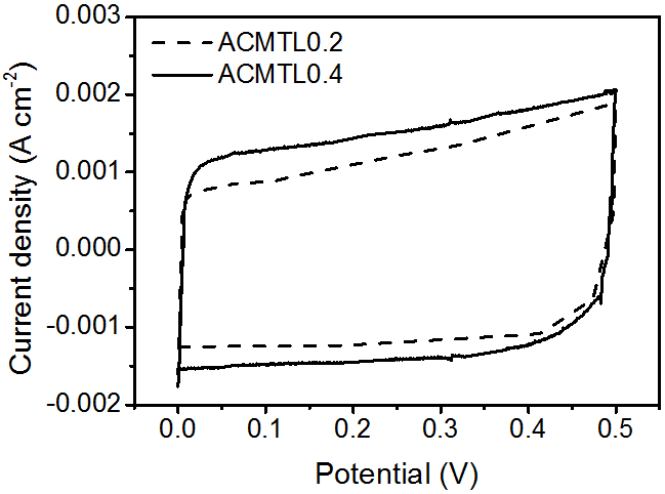

Figure 7: Cyclic Voltammetry curve of the ACMTLx electrodes

Further analysis, the energy and power densities were evaluated from Equations 6 and 7 to obtain 4.69-9.72Wh kg^{-1} and 33.84-70.12W kg^{-1}, respectively. These data were in terms of

Table 4: Electrochemical performance of some activated carbon precursors for supercapacitor electrode

Precursors	Electrode form	Activator agent	SBET (m^2 g^{-1})	D_{ave} (nm)	Csp (F g^{-1})	Electrolyte	Scan rate	Refs
Accacia leaves	Monolith	KOH	714	~2	113 (2E)	1 M H_2SO_4	1 mV s^{-1}	[17]
Albizia procera leaf	Powder	$NaHCO_3$	910	2.8	226 (3E)	1 M Na_2SO_4	5 mV s^{-1}	[18]
Orange peels	Powder	KOH	1577	2.07	165 (2E)	6 M KOH	10 mV s^{-1}	[53]
Ginkgo biloba leaves	Powder	KOH	835	1.48	281 (3E)	1 M H_2SO_4	10 mV s^{-1}	[48]
Mission grass	Monolith	NaOH	956	-	121 (2E)	1 M H_2SO_4	1 mV s^{-1}	[42]
Neem leaves	Powder	$ZnCl_2$	705	2.51	68 (2E)	1 M $LiClO_4$	10 mV s^{-1}	[54]
Saccharum bengalense leaves	Powder	$ZnCl_2$	2090	2.05	103 (2E)	1 M Li_2SO_4	2 mV s^{-1}	[55]
Tea waste	Powder	KOH	1058	1.66	133 (3E)	1 M H_2SO_4	5 mV s^{-1}	[56]
Commercial AC (Norit® SX2 POCH-Poland)	Powder	KOH	2800	-	202 (3E)	1 M H_2SO_4	1 mV s^{-1}	[57]
Commercial AC (Merck Chemical Reagent Company)	Powder	-	1771	1-2	235 (2E)	1 M H_2SO_4	-	[58]
Teak leaves	Monolith	KOH	490	2.39	280 (2E)	1 M H_2SO_4	1 mV s^{-1}	This work

activated carbon based-biomass electrode with densities of energy and power estimated as 9.2 Wh kg^{-1} and 48 W kg^{-1} respectively, based on the samples generated from ginkgo biloba leaves [48]. Subsequently, activated carbon electrodes from tobacco waste represented energy and power densities as 2.66Wh kg^{-1} and 51W kg^{-1} [49], correspondingly. Although, some energy density of activated carbon electrode originated from biomass have been reported, including palm empty fruit bunches (4.3Wh kg^{-1}) [50], tobacco rods (8,1Wh kg^{-1}) [51], fir sawdust (8,4Wh kg^{-1}) [52]. Table 4 shows the electrochemical performance comparison of ACMTL with respect to some activated carbon electrodes reported lasted, under various experimental parameter and textural properties, as well as measurement conditions. It performs that optimized ACMTL exhibits a high specific capacitance of 280F g^{-1}.

CONCLUSION

This study investigated the activated carbon monolith derived from novel biomass of fallen teak leaves by KOH under various concentration. The activated carbon monolith were synthesized through integrated pyrolysis of carbonization (N_2) and physical activation (CO_2). Based on the results and discussion, the ACMTL0.4 pore size distribution reflected a specific surface area of 489.81m^2 g^{-1} with total pore volume of 0.293cm^3 g^{-1}, while the average diameter in mesopores was 2.39nm. However, SEM images showed the macropores provide high ion transports. ACMTL0.4 with well-developed mesoporosity and large oxygen functional group presents suitable ion transport channels and good ion adsorption. These outcomes illustrated high specific surface area, appropriate pore size distribution, improved amorphous structure, as well as high oxygen functional group, exhibited comprehensive effects on electrochemical performance. Furthermore, the optimized ACMTL0.4 electrode possessed an advanced specific capacitance of 280F g^{-1} at 1mV s^{-1} with retained energy and power densities estimated at 9.72Wh kg^{-1} and 70.12W kg^{-1}, respectively in 1M H_2SO_4. This study significantly promotes the teak leaves as potential renewable and sustainable energy sources for energy storage materials.

ACKNOWLEGEMENTS

The authors would like to thank the DRPM Kemenristek-Dikti through the second year Project of PD (396/UN.19.5.1.3/PT.01.03/2020) with the title “High-density micro-and nano carbon fiber made from biomass based materials for supercapacitor electrodes”.

REFERENCES

1. Zakeri, B., Syri, S., (2015). Electrical energy storage systems: A comparative life cycle cost analysis. Renew. Sustain. Energy Rev., vol. 42, 569–596, DOI: 10.1016/j.rser.2014.10.011
2. Koohi-Fayegh, S., Rosen, M.A., (2020). A review of energy storage types, applications and recent developments. J. Energy Storage, vol. 27, 101047, DOI: 10.1016/j.est.2019.101047
3. Lefebvre, D., Tezel, F.H., (2017). A review of energy storage technologies with a focus on adsorption thermal energy storage processes for heating applications. Renew. Sustain. Energy Rev., vol. 67, 116–125, DOI: 10.1016/j.rser.2016.08.019
4. Khiari, B., Jeguirim, M., Limousy, L., Bennici, S., (2019). Biomass derived chars for energy applications. Renew. Sustain. Energy Rev., vol. 108, 253–273, DOI: 10.1016/j.rser.2019.03.057

5. Huang, J., Chen, L., Dong, H., Zeng, Y., Hu, H., Zheng, M., Liu, Y., Xiao, Y., Liang, Y., (2017). Hierarchical porous carbon with network morphology derived from natural leaf for superior aqueous symmetrical supercapacitors. Electrochim. Acta, vol. 258, 504–511, DOI: 10.1016/j.electacta.2017.11.092
6. Iqbal, M.Z., Zakar, S., Haider, S.S., (2020). Role of aqueous electrolytes on the performance of electrochemical energy storage device. J. Electroanal. Chem., vol. 858, 113793, DOI: 10.1016/j.jelechem.2019.113793
7. Yu, Y., Ye, Z., Chen, W., Wang, Q., Wang, H., Zhang, H., Peng, C., (2019). Plane tree bark-derived mesopore-dominant hierarchical carbon for high-voltage supercapacitors. Appl. Surf. Sci., vol. 507, 145190, DOI: 10.1016/j.apsusc.2019.145190
8. Zhao, C., Huang, Y., Zhao, C., Shao, X., Zhu, Z., (2018). Rose-derived 3D carbon nanosheets for high cyclability and extended voltage supercapacitors. Electrochim. Acta, vol. 291, 287–296, DOI: 10.1016/j.electacta.2018.09.136
9. Miller, E.E., Hua, Y., Tezel, F.H., (2018). Materials for energy storage: Review of electrode materials and methods of increasing capacitance for supercapacitors. J. Energy Storage, vol. 20, 30–40, DOI: 10.1016/j.est.2018.08.009
10. Fic, K., Platek, A., Piwek, J., Frackowiak, E., (2018). Sustainable materials for electrochemical capacitors. Mater. Today, vol. 21, 437–454, DOI: 10.1016/j.mattod.2018.03.005
11. Ratajczak, P., Suss, M.E., Kaasik, F., Beguin, F., (2018). Carbon electrodes for capacitive technologies. Energy Storage Mater, vol. 166, 126–145, DOI: 10.1016/j.ensm.2018.04.031
12. Inagaki, M., Konno, H., Tanaike, O., (2010). Carbon materials for electrochemical capacitors. J. Power Sources, vol. 195, 7880–7903, DOI: 10.1016/j.jpowsour.2010.06.036
13. Zhao, X., Chen, H., Kong, F., Zhang, Y., Wang, S., Liu, S., Lucia, L.A., Fatehi, P., Pang, H., (2019). Fabrication, characteristics and applications of carbon materials with different morphologies and porous structures produced from wood liquefaction: A review. Chem. Eng. J., vol. 364, 226–243, DOI: 10.1016/j.cej.2019.01.159
14. Jiang, C., Yakaboylu, G.A., Yumak, T., Zondlo, J.W., Edward, M., Wang, J., (2020). Activated carbons prepared by indirect and direct CO_2 activation of lignocellulosic biomass for supercapacitor electrodes. Renew. Energy, vol. 155, 38–52, DOI: 10.1016/j.renene.2020.03.111
15. Danish, M., Ahmad, T., (2018). A review on utilization of wood biomass as a sustainable precursor for activated carbon production and application. Renew. Sustain. Energy Rev., vol. 87, 1–21, DOI: 10.1016/j.rser.2018.02.003
16. Shanmuga, P.M., Divya, P., Rajalakshmi, R., (2020). A review status on characterization and electrochemical behaviour of biomass derived carbon materials for energy storage supercapacitors. Sustain. Chem. Pharm., vol. 16, 100243, DOI: 10.1016/j.scp.2020.100243
17. Taer, E., Natalia, K., Apriwandi, A., Taslim, R., Farma, R., (2020). The synthesis of activated carbon nanofiber electrode made from acacia leaves (Acacia mangium wild) as supercapacitors, Adv. Nat. Sci: Nanosci. Nanotechnol., vol. 11, 025007, DOI: 10.1088/2043-6254/ab8b60
18. Mohammedkhair, A.K., Aziz, M.A., Shah, S.S., Shaikh, M.N., Jamil, A.K., Qasem, M.A.A. Buliyaminu, I.A. Yamani, Z.H., (2020). Effect of an activating agent on the physicochemical properties and supercapacitor performance of naturally nitrogen-enriched carbon derived from Albizia procera leaves. Arabian Journal of Chemistry, vol. 13, 6161-6173, DOI: 10.1016/j.arabjc.2020.05.017
19. Jain, D., Kanungo, J., Tripathi, S.K., (2020). Enhancement in performance of supercapacitor using eucalyptus leaves derived activated carbon electrode with CH_3COONa and HQ electrolytes: A step towards environment benign supercapacitor. J. Alloys Compd., vol. 832, 154956, DOI: 10.1016/j.jallcom.2020.154956
20. Zhang, Y., Wang, C., Jiang, H., Wang, Q., Zheng, J., Meng, C., (2019). Cobalt-nickel silicate hydroxide on amorphous carbon derived from bamboo leaves for hybrid supercapacitors. Chem. Eng. J., vol. 375, 121938, DOI: 10.1016/j.cej.2019.121938
21. Wang, Y. Shao, C., Qiu, S., Zhu, Y., Qin, M., Meng, Y., Wang, Y., Chu, H., Zou, Y., Xiang, C., Zeng, J.L., Cao, Z., Xy, F., Sun, L., (2019). Nitrogen-doped porous carbon derived from ginkgo leaves with remarkable supercapacitance performance. Diam. Relat. Mater., vol. 98, 107475, DOI: 10.1016/j.diamond.2019.107475
22. Lu, Q., Zhou, S., Li, B., Wei, H., Zhang, D., Hu, J., Zhang, J., Liu, Q., Zhou, S., Li, B., Wei, H., Zhang, D., Hu, J., Zhang, L., Zhang, J., Liu, Q., (2020). Mesopore-rich carbon flakes derived from lotus leaves and it's ultrahigh performance for supercapacitors. Electrochim. Acta, vol. 333, 135481, DOI: 10.1016/j.electacta.2019.135481
23. Divya, P., Rajalakshmi, R., (2020). Renewable low cost green functional mesoporous electrodes from Solanum lycopersicum leaves for supercapacitors. J. Energy Storage, vol. 27, 101149, DOI: 10.1016/j.est.2019.101149
24. Ma, H., Liu, Z., Wang, X., Zhang, C., Jiang, R., (2017). Supercapacitive performance of porous carbon materials derived from tree leaves. J. Renew. Sustain. Energy, vol. 9, 044105, DOI: 10.1063/1.4997019

25. Liu, Y., Wang, Y., Zhang, G., Wang, D., Dong, Y., (2016). Preparation of activated carbon from willow leaves and evaluation in electric double-layer capacitors. Mater. Lett., vol. 176, 60–63, DOI: 10.1016/j.matlet.2016.04.065
26. Sagala, S (2015). Fostering Community Participation to Wildfire: Experiences from Indonesia, Elsevier Inc., DOI: 10.1016/B978-0-12-410434-1.00007-5
27. Taer, E., Mardiah, M.A., Sugianto, Juliani, R., Awitdrus, Farma, R., (2019). An introductory study on activated carbon monolith electrodes fabrication from teak leaf waste. J. Technomaterials Phys., vol. 1, 31–38
28. Wang, Y., Qu, Q., Gao, S., Tang, G., Liu, K., He, S., Huang, C., (2019). Biomass derived carbon as binder-free electrode materials for supercapacitors. Carbon, vol. 155, 706–726, DOI: 10.1016/j.carbon.2019.09.018
29. Moreno-Fernandez, G., Kunowsky, M., Lillo-rodenas, M.A., Ibanez, J., Rojo, J.M., (2017). New carbon monoliths for supercapacitor electrodes. looking at the double layer. ChemElectroChem, vol. 4, 1016–1025, DOI: 10.1002/celc.201600848
30. Taer, E., Taslim, R., Sugianto, Paiszal, M., Mukhlis., Mustika, W.S., Agustino., (2018). Meso-and microporous carbon electrode and its effect on the capacitive, energy and power properties of supercapacitor. Int. J. Power Electron. Drive Syst., vol. 9, 1263-1271, DOI: 10.11591/ijpeds.v9n3.pp1263-1271
31. Taer, E., Apriwandi., Handayani, R., Taslim, R., Awitdrus, Amri, A., Agustino., Iwantono, I., (2019). The Synthesis of Bridging Carbon Particles with Carbon Nanotubes from Areca catechu Husk Waste as Supercapacitor Electrodes. Int. J. Electrochem. Sci., vol. 14, 9436–9448, DOI: 10.20964/2019.10.34
32. Indonesia, D.J.K.I.R., (2015) Berita resmi paten sederhana seri-A. vol. 3, 1–3
33. Taer, E., Sugianto., Sumantre, M.A., Taslim, R., Iwantono, Dahlan, D., Deraman, M., (2014). Eggs Shell Membrane as Natural Separator for Supercapacitor Applications. Adv. Mater. Res., vol. 896, 66–69, DOI: 10.4028/www.scientific.net/AMR.896.66
34. Yang, X., Kong, L., Cao, M., Liu, X., Li, X., (2020). Porous nanosheets-based carbon aerogel derived from sustainable rattan for supercapacitors application. Ind. Crops Prod. 145 (2020) 112100, DOI: 10.1016/j.indcrop.2020.112100
35. Taer, E., Apriwandi., Yusriwandi., Mustika, W.S., Zulkifli., Taslim, R., Sugianto, Kurniasih B., Agustino., Dewi, P. (2018). Comparative study of CO_2 and H_2O activation in the synthesis of carbon electrode for supercapacitors. AIP Conf. Proc. 030036, 10.1063/1.5021229
36. Romero-rangel, C., Guillen-lopez, A., Mejía-mendoza, L.M., Robles, M., Espinosa-torres, N.D., Muniz, j., (2019). Approaches on the understanding of nanoporous carbon reactivity with polyatomic ions. Appl. Surf. Sci., vol. 495, 143392, DOI: 10.1016/j.apsusc.2019.07.134
37. Yahya, M.A., Al-qodah, Z., Ngah, C.W.Z, (2015). Agricultural bio-waste materials as potential sustainable precursors used for activated carbon production: A review. Renew. Sustain. Energy Rev., vol. 46, 218–235, DOI: 10.1016/j.rser.2015.02.051
38. Wei, X., Wei, J., Li, Y., Zou, H., (2019). Robust hierarchically interconnected porous carbons derived from discarded Rhus typhina fruits for ultrahigh capacitive performance supercapacitors. J. Power Sources, vol. 414, 13–23, DOI: 10.1016/j.jpowsour.2018.12.064
39. Xue, M., Lu, W., Chen, C., Tan, Y., Li, B., Zhang, C., (2019). Optimized synthesis of banana peel derived porous carbon and its application in lithium sulfur batteries. Mater. Res. Bull., vol. 112, 269–280, DOI: 10.1016/j.materresbull.2018.12.035
40. Mitravinda, T., Nanaji, K., Anandan, S., Jyothirmayi, A., Chakravadhanula, V.S.K., Sharma, C.S., Rao, T.N., (2018). Facile Synthesis of Corn Silk Derived Nanoporous Carbon for an Improved Supercapacitor Performance. J. Electrochem. Soc., vol. 165, 3369–3379, DOI: 10.1149/2.0621814jes
41. Ghosh, S., Santhosh, R., Jeniffer, S., Raghavan, V., Jacob, G., Nanaji, K., Kollu, P., Jeong, S.K., Grace, A.N., (2019). Natural biomass derived hard carbon and activated carbons as electrochemical supercapacitor electrodes. Sci. Rep., vol. 9, 16315, DOI: 10.1038/s41598-019-52006-x
42. Taer, E., Taslim, R., Mustika, W.S., Nurjanah, S., Yani, R.I., Sari, Y.P., Yusra, H., Awitdrus., Apriwandi., Agustino., Tahir, D., (2019). Preparation of mission grass flower-based activated carbon monolith electrode for supercapacitor application. Int. J. Electrochem. Sci., vol. 14, 7317–7331, DOI: 10.20964/2019.08.82
43. Kumar, K., Saxena, R.K., Kothari, R., Suri, D.K, Kaushik, K., Bohra, J.N, (1997). Correlation between adsorption and x-ray diffraction studies on viscose rayon based activated carbon cloth. Carbon, vol. 35, 1842–1844, DOI: 10./1016/S0008-6223(97)87258-2

44. Taer, E., Dewi, P., Syech, R., Taslim, R., Salomo., Susanti, Y., Purnama, A., Apriwandi., Agustino., Setiadi, R.N., (2018). The synthesis of carbon electrode supercapacitor from durian shell based on variations in the activation time. AIP Conf. Proc., vol. 1927, 030026, DOI: 10.1063/1.5021219
45. Song, X., Ma, X., Li, Y., Ding, L., Jiang, R., (2019). Tea waste derived microporous active carbon with enhanced double-layer supercapacitor behaviors. Appl. Surf. Sci., vol. 487, 189–197, DOI: 10.1016/j.apsusc.2019.04.277
46. Azwar, E., Adibah, W., Mahari, W., Huang, J., (2018). Transformation of biomass into carbon nanofiber for supercapacitor application: A review. Int. J. Hydrogen Energy, vol. 43, 20811–20821, DOI: 10.1016/j.ijhydene.2018.09.111
47. Taer, E., Taslim, R., Mustika, W.S., Kurniasih, B., Agustino., Afrianda, A., Apriwandi., (2018). Production of an activated carbon from a banana stem and its application as electrode materials for supercapacitors. Int. J. Electrochem. Sci., vol. 13, 8428–8439, DOI: 10.20964/2018.09.55
48. Zhu, X., Yu, S., Xu, K., Zhang, Y., Zhang, L., Lou, G., Wu, Y., Zhu, E., Chen, H., Shen, Z., Bao, B., Fu, S., (2018). Sustainable activated carbons from dead ginkgo leaves for supercapacitor electrode active materials. Chem. Eng. Sci., vol. 181, 36–45, DOI: 10.1016/j.ces.2018.02.004
49. Chen, H., Guo, Y., Wang, F., Wang, G., Qi, P., Guo, X., Dai, B., (2017). An activated carbon derived from tobacco waste for use as a supercapacitor electrode material. New Carbon Mater., vol. 32, 592–599, DOI: 10.1016/S1872-5805(17)60140-9
50. Farma, R., Deraman, M., Awitdrus, A., Talib, I.A., Taer, E., Basri, N.H., (2013). Preparation of highly porous binderless activated carbon electrodes from fibres of oil palm empty fruit bunches for application in supercapacitors. Bioresour. Technol., vol. 132, 254–261, DOI: 10.1016/j.biortech.2013.01.044
51. Zhao, Y., Lu, M., Tao, P., Zhang, Y., Gong, X., Yang, Z., Zhang, G., Li, H., (2016). Hierarchically porous and heteroatom doped carbon derived from tobacco rods for supercapacitors. J. Power Sources, vol. 307, 391–400, DOI: 10.1016/j.jpowsour.2016.01.020
52. Huang, Y., Liu, Y., Zhao, G., Chen, J.Y., (2017). Sustainable activated carbon fiber from sawdust by reactivation for high-performance supercapacitors. J. Mater. Sci., vol. 52, 478–488, DOI: 10.1007/s10853-016-0347-0
53. Ahmed, S., Rafat, M., Ahmed, A., (2018). Nitrogen doped activated carbon derived from orange peel for supercapacitor application. Adv. Nat. Sci: Nanosci. Nanotechnol., vol. 9, 035008, DOI: 10.1088/2043-6254/aad5d4
54. Ahmed, S., Parvaz, M., Johari, R., Rafat, M., (2018). Studies on activated carbon derived from neem (azadirachta indica) bio-waste, and its application as supercapacitor electrode. Mater. Res. Express, vol. 5, 045601, DOI: 10.1088/2053-1591/aab924
55. Rawal, S., Joshi, B., Kumar, Y., (2018). Synthesis and characterization of activated carbon from the biomass of Saccharum bengalense for electrochemical supercapacitors. J. Energy Storage, vol. 20, 418–426, DOI: 10.1016/j.est.2018.10.009.
56. Sankar, S., Talha, A., Ahmed, A., Inamdar, A.I., Im, H., Bin, Y., Lee, Y., Young, D., Lee, S., (2019). Biomass-derived ultrathin mesoporous graphitic carbon nano flakes as stable electrode material for high-performance supercapacitors. Mater. Des., vol. 169, 107688, DOI: 10.1016/j.matdes.2019.107688.
57. Lota, G., Centeno, T.A., Frackowiak E., Stoeckli, F, (2008). Improvement of the structural and chemical properties of a commercial activated carbon for its application in electrochemical capacitors. Electrochim. Acta, vol. 53, 2210–2216, DOI: 10.1016/j.electacta.2007.09.028.
58. Wang, W., Zhu, F., Jia, W., Wu, Y., Zhao, L., Yu, L., Chen, Y., Shen, Z, (2016). Electrochemical performance of activated carbons with different specific surface area as supercapacitor electrode materials. Int. J. Electrochem. Sci., vol. 11, 6688 –6695, DOI: 10.20964/2016.08.40

Paper submitted: 20.07.2020.
Paper accepted: 18.10.2020.